Frequency Dependent Indoor MIMO Channel Characterisation between 2 and 12 GHz Based on Full Spatial Correlation Matrices

Alexis P. García A. and Lorenzo Rubio
iTEAM Research Institute, Polytechnic University of Valencia -UPV, Valencia, Spain
Emails: algarar4@iteam.upv.es, lrubio@dcom.upv.es

Abstract— **The integration of wideband and multiple-input multiple-output (MIMO) radio technologies represents a powerful tool for different wireless communication standards. In the test process of these systems, new strategies for MIMO channel modelling and characterisation are necessary in order to investigate how the frequency band and the bandwidth affect the system performance. In this paper, a MIMO channel experimental characterisation based on full spatial correlation (FSC) MIMO matrices estimated from frequency domain measurements is presented. Measurements performed between 2 and 12 GHz in a stationary office scenario in both line-of-sight (LOS) and non-line-of-sight (NLOS) conditions are considered. Results show frequency dependency on the experimental MIMO channel characteristics under a high SNR regime, equal electric separation between array elements and isolation of the path loss effect. The ergodic and 1% outage capacities were reduced while the central frequency increases for different array configurations. Remarkable changes on the magnitude of the spatial correlation coefficients and on the MIMO system eigenvalues were observed for different band frequencies.**

Index Terms— **capacity, eigenvalues, full spatial correlation matrix, mobile radio channels, Multiple-Input Multiple-Output, space-time communications, spatial correlation**

I. Introduction

In wireless communications, space-time-frequency techniques are one of the most promising areas of innovation [1],[2]. In this way, multiple antenna systems, also known as multiple-input multiple-output (MIMO) systems, have proved highly efficient in the use of spectrum [3]. The main limitations in the application of these systems are the restrictions given by spatial correlations and rank deficiency of realistic MIMO channels [4],[5].

Therefore, MIMO channel characterisation is an important issue in order to assess a realistic MIMO system performance. In practice, to perform a MIMO channel characterisation it is often necessary to carry out a large number of measurements of the MIMO channel with slightly displaced arrays [6]-[9]. However, experimental studies based on measurements have usually investigated the MIMO channel characteristics focused on specific frequencies [6]-[14].

The new and constantly growing personal, local and metropolitan area wireless networks that consider MIMO technology will open a wide band of frequency options [15]-[20]. Therefore, it is necessary to study how the properties of the MIMO channel change with frequency. Recently, the impact of frequency has been studied in [21] at 2.55 and 5.25 GHz for an indoor scenario. This work found differences in the directional spread of the multipath components at both ends of the link, but left several questions open and did not show capacity results.

To illustrate how other frequency bands could impact the MIMO channel properties, we presented a previous work in [22], which is expanded in this paper. This paper presents a detailed experimental indoor MIMO channel characterisation using a procedure based on full spatial correlation (FSC) MIMO matrices and measurements performed between 2 and 12 GHz. The FSC MIMO matrices are estimated in different frequency bands from frequency domain complex samples obtained by means of modern wireless laboratory test equipment.

Spatial correlation, system eigenvalues, and MIMO capacity variations in terms of frequency are analysed. Each channel characteristic is studied under a high SNR regimen, equal electric separation between array elements in all frequencies, stationary indoor channel conditions and the isolation of the path loss effect.

The rest of the paper is organised as follows. Section II describes the environment, measurement procedure and post-processing applied to data, given details of the measurement setup, samples sequence segmentation, matrix normalisation and FSC MIMO matrix estimation. In Section III, we present the techniques used for synthetic MIMO channel generation, based on FSC MIMO matrices, and the formulation used for experimental MIMO channel analysis. The validation of the procedure is presented in Section IV. The results analysis is presented in Section V, where MIMO channel characteristics are compared for different frequency bands. Section VI concludes the paper.

This paper was presented in part at IEEE 66th Vehicular Technology Conference 2007, Baltimore, USA, 30 September - 3rd October, 2007.

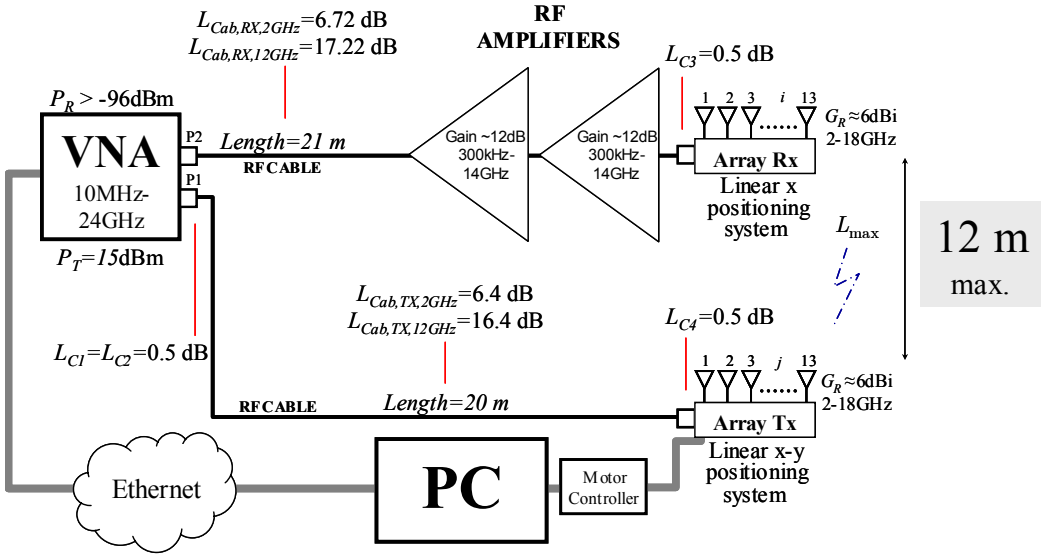

Figure 1. Measurement setup for MIMO channels using a vector network analyzer (VNA) taking into account the isolation of the path loss and a high SNR regime for indoor environments. The parameters L_x are related with losses for each component, P_x with powers and G_x with gains.

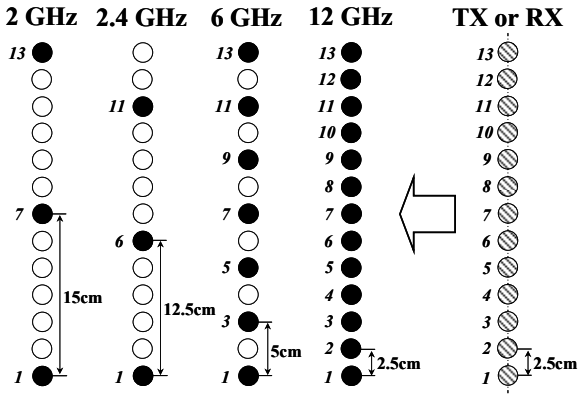

Figure 2. Virtual array configuration to perform measurements in different frequency bands using ULAs at both ends of the link.

II. Environment, Measurement, Post-processing and FSC MIMO Matrix Estimation

A. Environment description

The measurements were carried out in the iTEAM Research Institute at UPV, which were done at night, in absence of people and guaranteeing stationary conditions. The scenario included a room in LOS condition (laboratory room) and a corridor in NLOS (between an office room and the laboratory room), with wood made walls around, concrete columns and furniture. The receiver array (RX) was placed in the laboratory room and the transmitter array (TX) was placed in both that room and the adjacent corridor to obtain the two conditions with 10 different locations. The TX was located at a height of 1.7 m and the RX at 2 m. The maximum distance from the TX to RX was 12 m in order to guarantee a SNR higher than 15 dB in all conditions and frequency bands. For convenience, the TX was moved instead of the RX.

B. Measurement setup and procedure

To perform the measurement campaigns, we used a Vector Network Analyzer (VNA) with a dynamic range of 130 dB approximately, omnidirectional wideband biconical antennas (up to 18 GHz) in the TX and the RX side, wideband RF amplifiers in the RX side and very low attenuation cables (Fig. 1). The system resolutions were 10 μs of acquisition time per frequency bin, 50.01 kHz between frequency bins and a minimum of 2.5 cm between antenna elements.

For notation, we define the MIMO channel matrix by $\mathbf{H} \in \mathbb{C}^{N \times M}$, where M and N are the number of antenna elements at the transmitter and receiver, respectively, and $M \geq N$. The matrix $\mathbf{H}$ was measured in the frequency domain. It has used 200 MHz bandwidth (SPAN in the VNA) around each central frequency, f_c, in this case f_c={2,2.4,6,12} GHz, with 4000 frequency bin samples and 50 snapshots per location. The chosen frequency bands are included in the International Telecommunication Union (ITU) distribution frequencies for fixed and mobile terrestrial systems. It is worth to indicate that we have used 50 data acquisitions per frequency bin in order to average possible variability introduced by noise.

The antennas were mounted over a robotic precise linear positioning systems emulating virtual Uniform Lineal Arrays (ULA) without coupling effects. The virtual ULA arrays kept the same elements separation in terms of the wavelength, which were one wavelength for all frequencies using the minimum common step of 2.5 cm (Fig. 2). The filled black circles, which establish the one wavelength separations, were obtained by searching the correct elements over all 13 acquired data array elements (indicated as circles with oblique lines in Fig. 2). We only consider for subsequent analysis $M = N \leq 4$, in agreement with some current

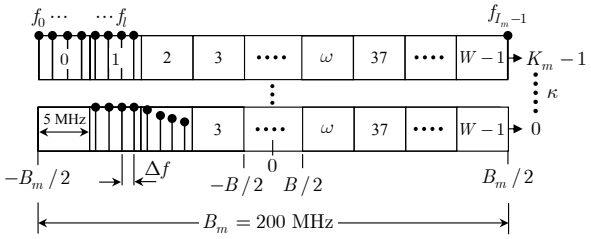

Figure 3. Samples and segmentation in the frequency domain used to calculate the entries of $\widehat{\mathbf{H}}$ based on the measured sequences $\widehat{H}_{ij}^{\kappa}[f_l]$ around f_c.

recommendations [15],[18]. We have established 30 cm as the maximum length for the ULAs (i.e., 2λ at 2 GHz).

The measurement procedure was controlled by a laptop remotely connected to the VNA and a motor controller. To measure relative effects versus frequency, all frequency bands data were collected simultaneously at the same array elements position.

C. Post-processing of data

With both the chosen environment and procedure described above, and applying Frobenius norm to the measured MIMO channel matrix, denoted by $\widehat{\mathbf{H}} \in \mathbb{C}^{N\times M}$, it is possible to eliminate the path loss effects for all frequency bands. In this way, we have assumed that the MIMO channel transfer matrix elements have identical average power [6].

To obtain the normalised non-frequency-selective stationary frequency domain MIMO channel, denoted by $\widehat{\mathbf{H}} \in \mathbb{C}^{N\times M}$, we use 40 consecutive windows of 5 MHz per frequency band and 50 snapshots. Primarily, we found in 200 MHz the stationary frequency selective channel coefficients $\widehat{H}_{ij}(f) \in \mathbb{C}$, where f indicates frequency domain. These coefficients are the entries of the matrix $\widehat{\mathbf{H}}$, in this case, the complex gain transmission coefficients from the *j*-th transmitting antenna to the *i*-th receiving antenna. It is worth indicating that for the considered indoor environment, it has verified a coherent bandwidth about 20 MHz. We use only a quarter of this bandwidth to obtain the stationary non-frequency selective channel coefficients $\hat{H}_{ij} \in \mathbb{C}$ from $\widehat{H}_{ij}(f)$.

To obtain $\widehat{\mathbf{H}}$, it has been used all l-th frequency bins and κ-th snapshots of the measured base-band discrete-complex sequences, $\widehat{H}_{ij}^{\kappa}[f_l]$, see Fig. 3, where $f_l = -B_m/2 + l\cdot\Delta f$, $l = \{0,1,\cdots,I_m-1\}$, and $\kappa = \{0,1,\cdots,K_m-1\}$. Here, B_m and Δf are the total bandwidth (200 MHz) and the system frequency domain resolution (50.01 kHz), respectively. I_m is the total number of frequency bin samples and K_m the total number of snapshot samples, i.e., I_m=4000 and K_m=50.

We divide $\widehat{H}_{ij}^{\kappa}[f_l]$ in W=40 frequency segments of B=5 MHz. This procedure was carried out by applying to $\widehat{H}_{ij}^{\kappa}[f_l]$ a sampled version of the rectangular unitary window

$$w(f) = \begin{cases} 1, & -B/2 \le f \le B/2, \\ 0, & otherwise, \end{cases} \tag{1}$$

as follows

$$\widehat{H}_{ij}^{\kappa,\omega}[f_{l'}] = \widehat{H}_{ij}^{\kappa}[f_{\omega R+l'}]\, w[f_{l'}], \tag{2}$$

where $f_{l'} = -B/2 + l'\cdot\Delta f$, $l' = \{0,1,\cdots,I-1\}$, $I = \lfloor I_m/W \rfloor$, $\omega = \{0,1,\cdots,W-1\}$, $i = \{1,2,\cdots,N\}$, $j = \{1,2,\cdots,M\}$ and choosing $R = I$ to obtain consecutive segments.

For $\widehat{H}_{ij}^{\kappa,\omega}[f_{l'}]$, $f_{l'}$ is the l'-th frequency bin sample inside the ω-th frequency segment at the κ-th snapshot sample.

Using (2), the ω-th averaged and normalised non-frequency selective MIMO channel transfer matrix, denoted by $\widehat{\mathbf{H}}_{\omega}^{[f_{l'}]} \in \mathbb{C}^{N\times M}$, is obtained calculating its entries as follows

$$\widehat{H}_{ij}^{\omega}[f_{l'}] = \left\langle \frac{\left(\widehat{H}_{ij}^{\kappa,\omega}[f_{l'}] - \left\langle \widehat{H}_{ij}^{\kappa,\omega}[f_{l'}] \right\rangle_{f_{l'}}\right)}{\sqrt{\mathrm{var}_{f_{l'}}\left(\widehat{H}_{ij}^{\kappa,\omega}[f_{l'}]\right)}} \right\rangle_{\kappa}, \tag{3}$$

where $\langle\cdot\rangle_{f_{l'}}$ and $\langle\cdot\rangle_{\kappa}$ denote sampled mean in $f_{l'}$ and κ domains, respectively, and $\mathrm{var}_{f_{l'}}(\cdot)$ denotes variance operator in $f_{l'}$ domain. By means of (3), the ω-th normalised non-frequency selective MIMO channel transfer matrix without path loss effects, denoted by $\widehat{\mathbf{H}}_{\omega} \in \mathbb{C}^{N\times M}$, is given by the square Frobenius norm [23] of $\widehat{\mathbf{H}}_{\omega}^{[f_{l'}]}$, applied to each l'-th frequency bin

$$\widehat{\mathbf{H}}_{\omega}^{[f_{l'}]} = \left((1/MNI) \sum_{l'=0}^{I-1} \left\| \widehat{\mathbf{H}}_{\omega}^{[f_{l'}]} \right\|_F^2 \right)^{-1/2} \widehat{\mathbf{H}}_{\omega}^{[f_{l'}]}, \tag{4}$$

where

$$\left\| \widehat{\mathbf{H}}_{\omega}^{[f_{l'}]} \right\|_F^2 = Tr\left[\left(\widehat{\mathbf{H}}_{\omega}^{[f_{l'}]} \right)^H \left(\widehat{\mathbf{H}}_{\omega}^{[f_{l'}]} \right) \right] = \sum_{i=1}^{N}\sum_{j=1}^{M} \left| \widehat{H}_{ij}^{\omega}[f_{l'}] \right|^2. \tag{5}$$

In (5) $Tr[\cdot]$ denotes trace and the superscript H indicates conjugate transpose. Note that in (4) the total channel components of the $\widehat{\mathbf{H}}_{\omega}$ matrix have unit power.

D. FSC MIMO matrix estimation

The FSC MIMO matrix, $\mathbf{R}_{\mathrm{MIMO}}$, is theoretically defined by [1]

$$\mathbf{R}_{\mathrm{MIMO}} \triangleq E\left[vec(\mathbf{H}) vec(\mathbf{H})^H \right], \tag{6}$$

where

$$vec(\mathbf{H})_{NM\times 1} = \\ = \left(H_{11}, H_{21}, .., H_{N1}, .., H_{1M}, H_{2M}, .., H_{NM}\right)^T,$$

$E[\cdot]$ is the expectation operator, and the superscript T indicates transpose. Note that $\mathbf{H} \in \mathbb{C}^{N\times M}$, with $M \geq N$. In (6) $\mathbf{R}_{\text{MIMO}} \in \mathbb{C}^{NM\times NM}$ is by definition a Hermitian and positive semidefinite matrix [23], and its entries follow

$$\left|R_{ij,\ell s}\right| = \left|E\left[H_{ij}H_{\ell s}^*\right]\right| \leq 1, \ \forall ij \neq \ell s.$$

We assume linearity between the MIMO channel entries, H_{ij}, stationary conditions, non-frequency selectivity, and a local area channel condition [24]. Hence, $\mathbf{R}_{\text{MIMO}}$ can be estimated by means of the Pearson's product moment correlation [23]. Then, using (4), for each frequency band, around of f_c, the $\mathbf{R}_{\text{MIMO}}$ matrix can be estimated by

$$\widetilde{\mathbf{R}}_{\text{MIMO}} = \frac{1}{WI}\sum_{\omega=0}^{W-1}\sum_{l'=0}^{I-1} vec\left(\widehat{\mathbf{H}}_{\omega}^{[f_{l'}]}\right) vec\left(\widehat{\mathbf{H}}_{\omega}^{[f_{l'}]}\right)^H, \quad (7)$$

where for our measurement setup configuration W =40, and I =100. Take into account we guarantee in all cases SNR>15 dB.

III. Experimental MIMO Channel Characterisation

To determine the cumulative distribution function (CDF) of the MIMO channel capacity from measurements, and thereby the outage capacity, thousands of MIMO channel samples are necessary.

Many works have been dedicated to develop new techniques to generate cross-correlated synthetic channels based in Gaussian samples [25]-[31], which is a useful task in the analysis of diversity systems. These works have led the way for practical analysis of MIMO channel characteristics in different environments, propagation conditions and array geometry configurations. One of the first practical works applying these techniques to MIMO was proposed by Kermoal *et al* in [9].

In general, the methods of generation of synthetic MIMO channels are based on the estimation of the covariance or correlation matrix of the MIMO system, which characterise the space-time variation of the channel [1]. Once the covariance or correlation matrix is estimated from a set of data, it is possible to use the Cholesky factorisation [23] to find the coloring matrix of the system [26]. This coloring matrix can be used to generate thousands of synthetic realisations of the space-time MIMO channel transfer matrix [9]. Finally, after the generation of an enough number of sampled MIMO matrices, it is possible to perform a reliable study of capacity, channel eigenvalues, and other MIMO channel characteristics, as it is suggested in [9].

A. Synthetic MIMO channel generation

From $\widetilde{\mathbf{R}}_{\text{MIMO}}$, it is possible to generate by simulation different realisations of $\mathbf{H}$ [9]. This procedure uses the Cholesky factorisation to decompose $\widetilde{\mathbf{R}}_{\text{MIMO}}$ as [23]:

$$\widetilde{\mathbf{R}}_{\text{MIMO}} = \mathbf{C}\mathbf{C}^H. \quad (8)$$

If the $\widetilde{\mathbf{R}}_{\text{MIMO}}$ matrix is positive definite, the $\mathbf{C}_{NM\times NM}$ matrix is a lower complex triangular matrix with real positive diagonal entries. Besides, this matrix is the unique lower triangular matrix satisfying (8).

The $\mathbf{C}$ matrix is the coloring matrix of the MIMO system and can be used to generate by simulation as many realisations of the MIMO channel as desired following [9],[25]-[31]:

$$vec(\widetilde{\mathbf{H}}) = \mathbf{C}\mathbf{a}, , \quad (9)$$

where $\widetilde{\mathbf{H}} \in \mathbb{C}^{N\times M}$ is the synthetic MIMO channel transfer matrix,

$$\mathbf{a}_{NM\times 1} = \left(\alpha_{11}, \alpha_{21}, \ldots, \alpha_{N1}, \ldots, \alpha_{1M}, \alpha_{2M}, \ldots, \alpha_{NM}\right)^T,$$

and α_{ij} are zero-mean complex independent identically distributed (i.i.d) random variables.

Equations (8) and (9) permit to generate the cross-correlated $N \times M$ complex normal random variables of the entries of $\widetilde{\mathbf{H}}$, which have the specific correlation matrix $\widetilde{\mathbf{R}}_{\text{MIMO}}$.

The main limitation of this procedure is that the experimental correlation matrix $\widetilde{\mathbf{R}}_{\text{MIMO}}$ must be a Hermitian positive definite matrix to apply the Cholesky factorisation. Provided that correlation matrices derived from measurements or synthetic samples are not always guaranteed to be positive definite (see e.g., [32],[33]), the $\mathbf{C}$ matrix does not always exist, making the Cholesky factorisation unsuitable. This problem happens usually for large MIMO arrays, which is not the case in this paper due to $M = N \leq 4$. For large-scale arrays, the non-positiveness can be solved applying other techniques, for example the covariance matrix estimation given in [34].

B. Experimental MIMO channel capacity

The capacity analysis showed here will be related with the capacity found by means of the normalized non-frequency-selective stationary frequency domain MIMO synthetic channel, $\widetilde{\mathbf{H}}$. We will also show, in the next section, comparative results between $\widehat{\mathbf{H}}_{\omega}$ and $\widetilde{\mathbf{H}}$ in order to validate the procedure.

With one hundred thousands samples generated for $\widetilde{\mathbf{H}}$, we can compare the performance of the MIMO system in different conditions and frequency bands. In this paper, we restricting our analysis to frequency flat-fading channels in each frequency band and assuming that the channel is unknown at the TX and perfectly known at the RX. Under these conditions, the experimental MIMO capacity, denoted by $\tilde{C}$, is given by [1].

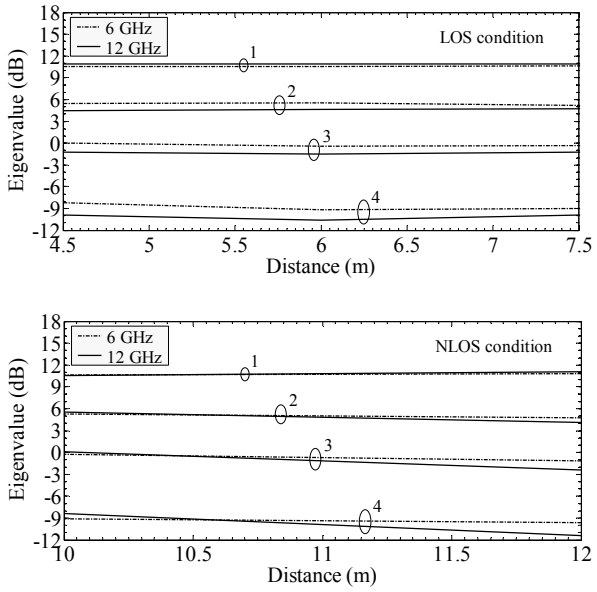

Figure 4. Path loss effect isolation: mean local eigenvalues variations vs. distance for (4,4), one wavelength element separations, 6 and 12 GHz, in LOS and NLOS. The numbers 1-4 means $\tilde{\lambda}_1$, $\tilde{\lambda}_2$, $\tilde{\lambda}_3$ and $\tilde{\lambda}_4$, where $\tilde{\lambda}_1 > \tilde{\lambda}_2 > \tilde{\lambda}_3 > \tilde{\lambda}_4$.

$$\tilde{C} = \log_2 \left\{ \det \left(\mathbf{I}_M + \frac{P_{TX}}{M\sigma^2} \widetilde{\mathbf{H}}^H \widetilde{\mathbf{H}} \right) \right\}, \qquad (10)$$

where P_{TX} is the total transmit power, σ^2 is the power receive noise and $\mathbf{I}_M$ is a $M \times M$ identity matrix. On the other hand, the outage capacity at 1%, $\tilde{C}_{out,1\%}$ can be defined by $\mathrm{P}\left[\tilde{C} \le \tilde{C}_{out,1\%}\right] = 1\%$, where $\mathrm{P}[.]$ indicates probability.

D. Experimental MIMO systems eigenvalues and spatial correlation coefficients

The random coefficients $\tilde{\lambda}_i \in \mathbb{R}_+$ are the eigenvalues of $\widetilde{\mathbf{H}}^H \widetilde{\mathbf{H}}$, also known as MIMO system eigenvalues [1]. Considering $\widetilde{\mathbf{H}}$ a random matrix that reflect all the MIMO channel characteristics (spatial correlation, double scattering, keyhole, pinhole effects, etc. [5]), the random eigenvalues of $\widetilde{\mathbf{H}}^H \widetilde{\mathbf{H}}$ can reflect any of those characteristics, including others channel degenerations, as space-frequency degeneration.

On the other hand, for spatial correlation analysis, we will consider the magnitude of the complex correlation coefficients of $\widetilde{\mathbf{R}}_{\mathrm{MIMO}}$, $\tilde{R}_{ij,\ell s}$, i.e., the sampled mean $\left\langle \left| \tilde{R}_{ij,\ell s} \right| \right\rangle_{j=s}$ for the nearest RX antenna elements with $i = 1$, and $\ell = 2$.

IV. Validation of The Experimental Procedure

To assure a fair comparison in different frequencies with isolation of the path loss effect, we show in Fig. 4 the mean eigenvalues, $\left\langle \tilde{\lambda}_i \right\rangle$, variations while distance increases, in this case for 6 and 12 GHz in a $(M = 4, N = 4)$ array configuration in LOS and NLOS. As expected, the eigenvalues remain mostly constant versus distance, with only a slow decrease in the smallest eigenvalues for longer ranges in NLOS condition.

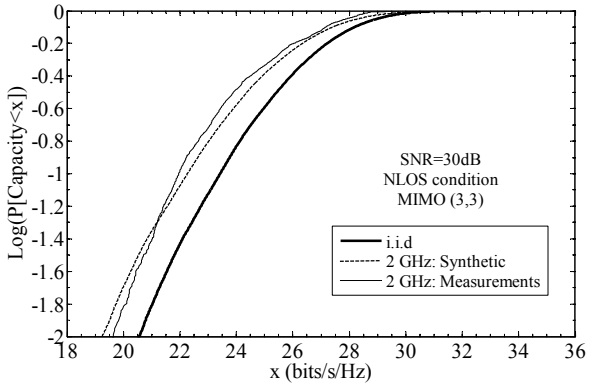

Figure 5. CDF of the MIMO capacity for (3,3), one wavelength element separations, and 2 GHz, for the synthetic MIMO channel $\widetilde{\mathbf{H}}$ and the measured MIMO channel $\widehat{\mathbf{H}}_\omega$.

On the other hand, Fig. 5 shows comparative results of the experimental CDF of the MIMO capacity, considering measurements and the synthetic MIMO channel, for a (3,3) case in NLOS at 2 GHz with a SNR of 30 dB. We used all samples (locations in NLOS, windows and frequency bin samples) of the measured matrix $\widehat{\mathbf{H}}_\omega$, from (4), and the synthetic generated matrix $\widetilde{\mathbf{H}}$, from (9), with one hundred thousands samples.

Since the path loss effect is isolated for $\widetilde{\mathbf{H}}$ (Fig. 4), and we found a good fit between the CDF capacities of $\widetilde{\mathbf{H}}$ and $\widehat{\mathbf{H}}_\omega$ (Fig. 5), it is clear that the procedure proposed in Section II and III is valid for the indoor MIMO channel characterisation between 2 and 12 GHz.

V. Results Analysis

In this section, we compare the performance of the MIMO system in different propagation conditions and frequency bands. We analyze $\tilde{C}$, $\tilde{C}_{out,1\%}$, $\tilde{\lambda}_i$ and the coefficients $\left\langle \left| \tilde{R}_{ij,\ell s} \right| \right\rangle_{j=s}$, taking into account only in the RX the correlation coefficients between nearest array elements (one wavelength) and other separations for all frequency bands.

In relation to the ideal (i.i.d) and the correlated MIMO channel from different frequency bands, the study has shown changes in the system capacity, in every (M, N) case. The (3,3) configuration shows a clear frequency dependence in the CDF of the capacity $\tilde{C}$ (see the Fig. 6). When the frequency increases, the capacity drops. This reduction happens in both propagation conditions, with smaller differences for NLOS. Besides, the reduction between the nearest frequency bands (i.e., 2 and 2.4 GHz) is not noticeable for NLOS cases.

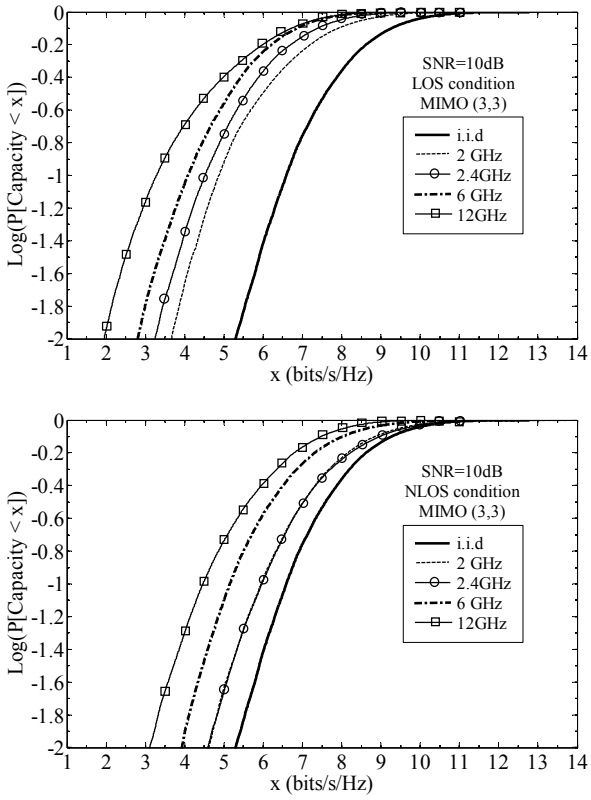

Figure 6. CDF of the capacity, $\tilde{C}$, for (3,3) with one wavelength element separations, in LOS and NLOS, for four different frequency bands and the i.i.d case.

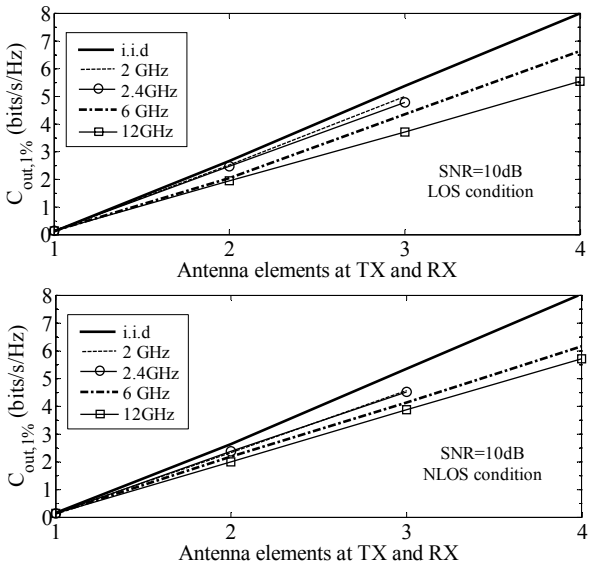

Figure 7. 1% outage capacity, $\tilde{C}_{out,1\%}$, for (1,1), (2,2), (3,3) and (4,4) with one wavelength element separations, in LOS and NLOS for four different frequency bands and the i.i.d case.

Fig. 7 shows the 1% outage capacities, $\tilde{C}_{out,1\%}$, obtained in LOS and NLOS conditions in each frequency band for (1,1), (2,2), (3,3) and (4,4) cases with a SNR of 10 dB. Note that the designed ULAs can only offer until (3,3) configurations for 2 and 2.4 GHz (see Fig. 2).

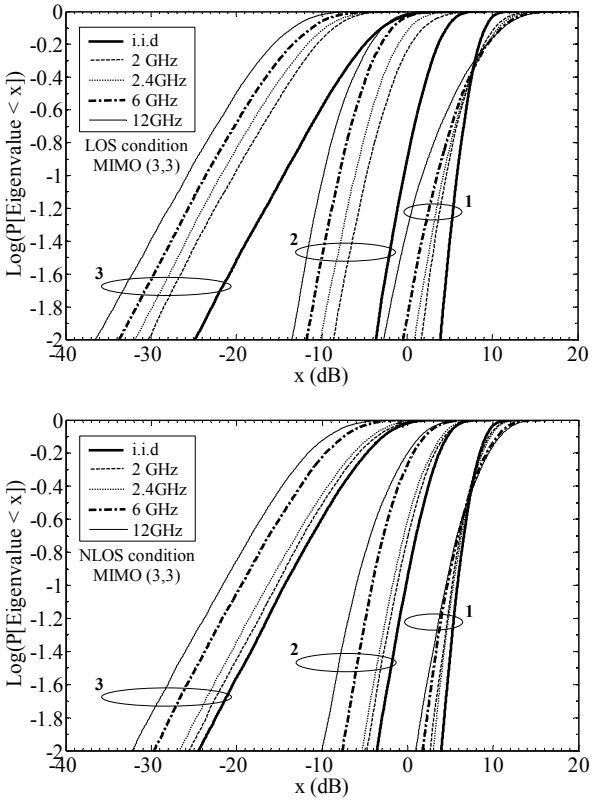

Figure 8: Eigenvalues CDF for a (3,3) array configuration, one wavelength element separations in LOS and NLOS. The numbers 1-3 means $\tilde{\lambda}_1$, $\tilde{\lambda}_2$, and $\tilde{\lambda}_3$, where $\tilde{\lambda}_1 > \tilde{\lambda}_2 > \tilde{\lambda}_3$.

We found remarkable differences between the ideal case (i.i.d) and measurements in LOS and NLOS for all (M,N) cases. In LOS, these differences are among 0.5 and 2 bits/s/Hz for (3,3), and among 1.5 and 2.5 bits/s/Hz for (4,4). In NLOS, the relative capacity reductions are slightly smaller than LOS, and the differences between frequency bands are smaller. Thus, the reductions were among 1 and 1.5 bits/s/Hz for (3,3), and among 1.7 and 2.2 bits/s/Hz for (4,4).

The experimental 1% outage capacity results (Fig. 7) show that the relative reductions with frequency are not linear when the number of antenna elements increase. Besides, in the same way as in Fig.6, the capacity reduction between the nearest frequency bands is not noticeable for NLOS cases, even for different array configurations. It is worth to indicate that we also found relative capacity reduction for the 10% outage capacity in every (M,N) array configuration [22].

On the other hand, Fig. 8 shows the frequency effects reflected in the CDF of the eigenvalues $\tilde{\lambda}_i$ for the same cases of Fig. 6. The reduction in the smallest eigenvalues, $\tilde{\lambda}_2$ and $\tilde{\lambda}_3$, are higher than in the biggest eigenvalue, $\tilde{\lambda}_1$, which happens in LOS and NLOS, but in less proportion for NLOS and at 2 and 2.4 GHz. The most important result from Fig. 8 is that the distribution of $\tilde{\lambda}_1$ change with frequency, but around $\log\left(\mathrm{P}\left[\tilde{\lambda}_1 \le \tilde{\lambda}_{1,50\%}\right] = 50\%\right)$

TABLE I.
CORRELATION COEFFICIENTS IN LOS

d (cm)	2 GHz	2.4 GHz	6 GHz	12 GHz
	Mean	Mean	Mean	Mean
2.5	0.945	0.938	0.921	***0.979***
5	0.797	0.729	***0.785***	-
7.5	0.395	0.487	-	-
10	0.387	0.396	-	-
12.5	0.331	***0.452***	-	-
15	***0.326***	-	-	-

TABLE II.
CORRELATION COEFFICIENTS IN NLOS

d (cm)	2 GHz	2.4 GHz	6 GHz	12 GHz
	Mean	Mean	Mean	Mean
2.5	0.820	0.886	0.924	***0.870***
5	0.579	0.717	***0.780***	-
7.5	0.573	0.556	-	-
10	0.275	0.453	-	-
12.5	0.262	***0.425***	-	-
15	***0.283***	-	-	-

the value remains mostly constant in LOS and NLOS.

Frequency dependent effects are also reflected in the correlation coefficients $\left\langle \left| \tilde{R}_{ij,\ell s} \right| \right\rangle_{j=s}$ (Table I and Table II). For fair comparisons between different frequency bands, the spatial correlation coefficients $\left\langle \left| \tilde{R}_{1j,2s} \right| \right\rangle_{j=s}$ should be observed at one wavelength (in bold), and for other comparisons, can be considered the antenna element separation (*d*). As expected and according to the last capacity results, the correlation coefficient increases with frequency, with fewer differences between 2 and 2.4 GHz.

To conclude, the experimental frequency band dependences obtained in this work can be explained due to differences in the spatial characteristics of the MIMO channel. From a physical point of view, these effects are related to a change on the angular spread of the MIMO channel for different frequency bans [21].

VI. CONCLUSION

We have researched the impact of frequency on the MIMO channel characteristics for an indoor environment, and implemented a measurement procedure to do a fair comparison in four different frequency bands in a high SNR regime. The results presented in this work are useful for test and development of wireless systems considering MIMO operating in the analysed frequency bands.

The results show that the CDF of the capacity for an indoor MIMO system has frequency band dependence. Compared with the i.i.d channel for $M = N = \{2, 3, 4\}$ cases, the 1% outage capacities were reduced while the frequency was increased. The maximum relative capacity reduction was for a $M = N = 4$ case at 12 GHz. These results were found in LOS and NLOS conditions. These changes versus frequency were related to both the increase of the receiver spatial correlation coefficients and the reduction in the MIMO system eigenvalues while the frequency grows. The reductions in eigenvalues were higher for the smallest eigenvalues and considerably lower for the highest eigenvalue, showing modifications with frequency in the distribution of the highest eigenvalue. The differences in capacity, eigenvalues, and spatial correlation coefficients were lower between 2 and 2.4 GHz, and for NLOS cases.

ACKNOWLEDGMENT

This work was supported by the AlBan Programme, the European Union Programme of High Level Scholarships for Latin America, scholarship No. E04D044088CO.

REFERENCES

[1] A. Paulraj, R. Nabar and D. Gore, *Introduction to space-time wireless communications*, Cambridge University Press, 2003.

[2] V. Kühn, *Wireless communications over MIMO channels: applications to CDMA and multiple antenna systems,* John Wiley & Sons Ltd, 2006.

[3] G. J. Foschini, and M.J. Gans, "On limits of wireless communications in a fading environment when using multiple antennas", *Wireless Personal Commun*., vol. 6, no.3, pp.311-315, 1998.

[4] D. Chizhik, F. Rashid-Farrokhi, J. Ling and A. Lozano, "Effect of antenna separation on the capacity of BLAST in correlated channels", *IEEE Commun. Letters*, vol. 4, no. 11, pp.337-339, November 2000.

[5] H. Shin, and J. H. Lee, "Capacity of multiple-antenna fading channels: spatial fading correlation, double scattering, and keyhole", *IEEE Trans. on Information Theory*, vol. 49, no. 10, pp. 2636-2647, October 2003.

[6] D. Chizhik, et al, "Multiple-input-multiple-output measurements and modeling in Manhattan", *IEEE J. on Selected Areas in Commun.*, vol. 21, no. 3, pp. 321-331. April 2003.

[7] P. Kyritsi, D. C. Cox, R. A. Valenzuela, and P. W. Wolniansky, "Correlation analysis based on MIMO channel measurements in an indoor environment", *IEEE J. on Selected Areas in Commun*., vol. 21, no. 5, pp. 713-720, June 2003.

[8] A. F. Molisch, M. Steinbauer, M. Toeltsch, E. Bonek, and R. S. Thomä, "Capacity of MIMO systems based on measured wireless channels", *IEEE J. on Selected Areas in Commun.*, vol. 20, no. 3, pp. 561-569, April 2002.

[9] J. P. Kermoal, L. Schumacher, K. I. Pedersen, P. E. Mogensen, and F. Frederiksen, "A stochastic MIMO radio channel model with experimental validation", *IEEE J. on Selected Areas in Commun.*, vol. 20, no. 6, pp. 1211-1226, August 2002.

[10] D. S. Baum, et al., "Measurements and characterization of broadband MIMO fixed wireless channels at 2.5 GHz", *Proceedings of ICPWC'00*, Hyderabad, December 2000.

[11] J. W. Wallace and M. A. Jensen, "Characteristics of measured 4×4 and 10×10 MIMO wireless channel data at 2.4-GHz", *IEEE Antennas and Propagation Society International Symposium*, Boston, July 2001.

[12] J. W. Wallace and M. A. Jensen, "Measured characteristics of the MIMO wireless channel", *IEEE 54th Vehicular Technology Conference - VTC Fall 2001*, Atlantic City, October 2001.

[13] J. P. Kermoal, et. al., "Experimental investigation of correlation properties of MIMO radio channels for indoor picocell scenarios", *IEEE 52nd Vehicular Technology Conference - VTC Fall 2000*, Boston, September 2000.
[14] J. P. Kermoal, et. al., "Smart antennas cluster year 2000 report", *IST-1999-11729 METRA Project*, In: http://www.ist-imetra.org/metra/papers/
[15] "Multiple-Input Multiple-Output in UTRA", 3GPP TR25.876 V1.8.0., Oct. 2005.
[16] "Spatial channel model for multiple input multiple output (MIMO) simulations", 3GPP TR 25.996 V7.0.0:, June 2007.
[17] "Part 11: Wireless LAN medium access control (MAC) and physical layer (PHY) specifications", IEEE P802.11n, D3.00, Sept. 2007.
[18] "Part 16: Air interface for fixed broadband wireless access systems", IEEE Std 802.16 2004, Oct. 2004.
[19] A. F. Molisch, et all, "A comprehensive standardized model for ultrawideband propagation channels", *IEEE Trans. on Antennas and Propagation"*, vol. 54, no. 11, pp. 3151-3166, November 2006.
[20] P. Pagani, and P. Pajusco, "Modeling the space-and time-variant ultra-wideband propagation channel", *IEEE International Conference on Ultra-Wideband,* September 2006.
[21] E. Bonek, et al, "Indoor MIMO measurements at 2.55 and 5.25 GHz - a comparison of temporal and angular characteristics." *Procc. of the IST Mobile Summit*, Myconos, June 2006.
[22] A. P. García and L. Rubio "Frequency impact on the indoor MIMO channel capacity between 2 and 12 GHz". *IEEE 66th Vehicular Technology Conference – VTC Fall 2007*, Baltimore, October 2007.
[23] C. D. Mayer, *Matrix analysis and applied linear algebra,* Society for Industrial and Applied Mathematics, 2000.
[24] G. D. Durgin, *Space-time wireless channels*, Pearson Education, Inc., NJ, US, 2003.
[25] R. B. Ertel and J.H. Reed, "Generation of two equal power correlated Rayleigh fading envelopes", *IEEE Commun. Letters*, vol. 2, no. 10, pp. 276-278, October 1998.
[26] N. C. Beaulieu, "Generation of correlated Rayleigh fading envelopes", *IEEE Commun. Letters*, vol. 3, no. 6, pp. 172-174, June 1999.
[27] B. Natarajan, C.R. Nassar and V. Chandrasekhar, "Generation of correlated Rayleigh fading envelopes for spread spectrum applications", *IEEE Commun. Letters*, vol. 4, no. 1, pp. 9-11, January 2000.
[28] N. C. Beaulieu and M.L. Merani, "Efficient simulation of correlated diversity channels", *IEEE Wireless Commun. and Networking Conference – WCNC 2000,* Chicago, September 2000.
[29] Q. T. Zhang, "A decomposition technique for efficient generation of correlated Nakagami fading channels", *IEEE J. Select. Areas Commun.*, vol. 18, no. 11, pp. 2385-2392, November 2000.
[30] K. Zhang, Z. Song and Y. L. Guan, "Simulation of Nakagami fading channels with arbitrary cross-correlation and fading parameters", *IEEE Trans. on Wireless Commun.*, vol. 3, no. 5, pp. 1463-1468, September 2004.
[31] K. E., Baddour and N. C. Beaulieu, "Accurate simulation of multiple cross-correlated Rician fading channels", *IEEE Trans. on Commun.*, vol. 52, no. 11 pp. 1980-1987, November 2004.
[32] Y. I. Abramovich, N. K Spencer and A. Y. Gorokhov, "Detection-estimation of more uncorrelated Gaussian sources than sensors in nonuniform linear antenna arrays - Part I: Fully augmentable arrays", *IEEE Trans. on Signal Processing*, vol. 49, no. 5, pp. 959-971, May 2001.
[33] S. Sorooshyari and D. G. Daut, "On the generation of correlated Rayleigh fading envelopes for accurate simulation of diversity channels", *IEEE Trans. on Commun.*, vol. 54, no. 8, pp. 1381-1386, August 2006.
[34] J. Schäfer, and K. Strimmer, "A Shrinkage approach to large-scale covariance matrix estimation and implications for functional genomics', *Statistical Applications in Genetics and Molecular Biology*, vol. 4, no. 1, 2005.

Alexis Paolo García Ariza received his M.S. degree in electronic engineering from the Industrial University of Santander (UIS), Bucaramanga, Colombia, in 2002, and DEA in telecommunications from Polytechnic University of Valencia (UPV), Valencia, Spain, in 2007. He is a Ph.D. student in telecommunication at UPV since 2004, with the support of the European AlBan Programme.

He was with RadioGIS research group at UIS between 2002 and 2004, where he developed investigations in propagation models applied to Andean conditions, and designing radio network planning tools based on Geographic Information Systems (GIS). He is currently a Research Engineer with the iTEAM Research Institute at UPV, Valencia, Spain. His research is focused on modelling, simulation and measurement of wireless channels, with special interest in wideband MIMO channels, MIMO system performance and Ultra Wideband (UWB) channels. He was a guest researcher at Mobile Communications Group, University of Agder, Grimstad, Norway, in 2007, where he developed investigations in perfect modelling and simulation of MIMO channels using real-world measurement data.

Mr. García was IEEE Student-member between 2000 and 2002, and IEEE Antennas and Propagation Society Member between 2002 and 2003. He was a member of the local committee of the IEEE 3rd International Symposium on Wireless Communication System (ISWCS 2006), president of the IEEE Student Branch - UIS, year 2001, and chairman of the First Electrical and Electronics Engineering International Conference (CIIEE 2000).

Lorenzo Rubio received the Telecommunication Engineering and the Ph.D degrees from the Universidad Politécnica de Valencia (UPV), Spain, in 1996 and 2004 respectively. In 1996, he joined the Communications Department of the UPV, where he is now Associate Professor of wireless communications. He is a member of the Radio and Wireless Communications Group (RWCG) of the Telecommunications and Multimedia Applications Research Institute (iTEAM).

His main research interests are related to wireless communications. Specific current research topics include radiowave propagation, measurement and mobile time-varying channels modelling in vehicular applications, ultra-wideband (UWB) communication systems, MIMO systems and equalization techniques in digital wireless systems.

Dr. Rubio was awarded with the Ericsson Mobile Communications prize from the Spanish Telecommunications Engineering Association for his study on urban statistical radiochannel characterisation applied to wireless communications.